

# A Biomechanical Study of the Charleston Brace for the Treatment of Scoliosis

Julien Clin, MScA,\*† Carl-Éric Aubin, PhD, PEng,\*† Stefan Parent, MD, PhD,†  
and Hubert Labelle, MD†

**Study Design.** A biomechanical study of the Charleston brace.

**Objective.** To model the nighttime Charleston brace treatment and study its biomechanical action.

**Summary of Background Data.** The Charleston brace has been proposed as an alternative to the traditional daytime thoracolumbosacral orthosis for the treatment of moderate scoliotic deformities. It is worn at night and imposes a supine side-bending to reduce the major scoliotic curve. The biomechanics of the Charleston brace is still poorly understood.

**Methods.** The geometry of the spine, pelvis, rib cage, and of the external trunk surface of 2 scoliotic patients were acquired using a 3-dimensional multiview radiograph reconstruction technique and surface topography. A finite element model of each patient's trunk was created. Two sets of mechanical properties (stiff and normal) of the spine were tested. For each case, the transition from standing to supine position was first simulated by modifying the direction of the gravity forces acting on the patients' spine. Supine bending was simulated by applying a lateral displacement on the first thoracic vertebra. A custom-fit Charleston brace was modeled and positioned on the patient model. Tension was applied in the straps. Efficiency of the simulated Charleston braces was studied by computing geometrical corrections and effects on the internal stresses of the spine.

**Results.** The reduction of the major scoliotic curve varied between 58% and 97% and was in the range of published clinical data. Internal compressive stresses up to 1 MPa were generated on the convex side of the major scoliotic curve and tensile stresses up to 1 MPa on its concavity. In contrast, increased compressive stresses were exerted on the concavity of the secondary curves and added tensile stresses in their convexity.

**Conclusion.** This study quantified the Charleston brace's biomechanical effect, which consists in inverting the asymmetrical compressive loading in the major scoliotic curve. It also highlighted that the Charleston brace

worsens the asymmetrical compressive loading in the compensatory curves. The finite element model developed could help studying different brace designs and optimizing brace efficiency.

**Key words:** scoliosis, Charleston brace, finite element model, biomechanics. **Spine 2010;35:E940–E947**

Scoliosis is a 3-dimensional deformity of the spine and the rib cage. For small and moderate curves, bracing is the most common treatment. Different bracing systems exist; the most frequently used being the thoracolumbosacral orthoses (TLSOs) that are generally worn almost full-time. The Boston brace in North America and the Chêneau brace in Europe are examples of commonly used TLSOs. An alternative to the TLSO is the nighttime Charleston Brace, introduced in 1990 by Price *et al.*<sup>1</sup> Its action principle is to impose a supine side-bending to the patient trunk in the direction of the major scoliotic curve to reduce it.<sup>2</sup> The clinical efficiency of the Charleston brace to prevent the progression of the scoliotic curves has been demonstrated<sup>1,3,4</sup> and compared with conventional TLSOs.<sup>5–7</sup> Katz *et al.*<sup>7</sup> and Howard *et al.*<sup>6</sup> concluded that the TLSOs are more efficient than the Charleston brace, whereas Gepstein *et al.*<sup>5</sup> found no significant difference.

The Charleston brace designers have underlined that the factors contributing to the efficiency of nighttime side-bending are unclear.<sup>2</sup> Stretching the concavity of the curvature and possibly a physiologic contracture on the convexity seems to play a role, but that has not been proven. In theory, the brace should add opposite tensile and compression forces to the vertebral epiphyses compared with the forces acting in an upright posture.

To better understand the biomechanics of a TLSO, finite element (FE) models have been used. The Milwaukee brace<sup>8</sup> and the Boston brace<sup>9,10</sup> have been simulated by directly applying forces on a FE model of the trunk. The optimal forces to correct scoliotic deformities have been studied.<sup>11–13</sup> Recently, a more realistic model to simulate a TLSO treatment has been proposed.<sup>14</sup> Instead of directly applying forces on a FE model of the trunk, a TLSO was explicitly modeled, and its action on the patient simulated using a contact interface.

The Charleston brace treatment, however, has never been simulated. Consequently, the aim of this study was to model the Charleston brace treatment to study its biomechanical action and to verify whether it really adds opposite tensile and compression forces to the vertebral

From the \*Department of Mechanical Engineering, École Polytechnique de Montréal; and †Sainte-Justine University Hospital Center, Montréal, Québec, Canada.

Acknowledgment date: May 20, 2009. Revision date: September 18, 2009. Acceptance date: October 3, 2009.

The manuscript submitted does not contain information about medical device(s)/drug(s).

Funding was received for research from Natural Sciences and Engineering Research Council of Canada. No benefits in any form have been or will be received from a commercial party related directly or indirectly to the subject of this manuscript.

Supported by the Natural Sciences and Engineering Research Council of Canada.

Address correspondence and reprint requests to Carl-Éric Aubin, PhD, PEng, Full Professor, Canada Research Chair "CAD Innovation in Orthopedic Engineering" and NSERC-Medtronic Industrial Research Chair in Spine Biomechanics, Ecole Polytechnique, Department of Mechanical Engineering, P.O. Box 6079, Station "Centre-Ville," Montréal, Québec, H3C 3A7 Canada; E-mail: carl-eric.aubin@polymtl.ca

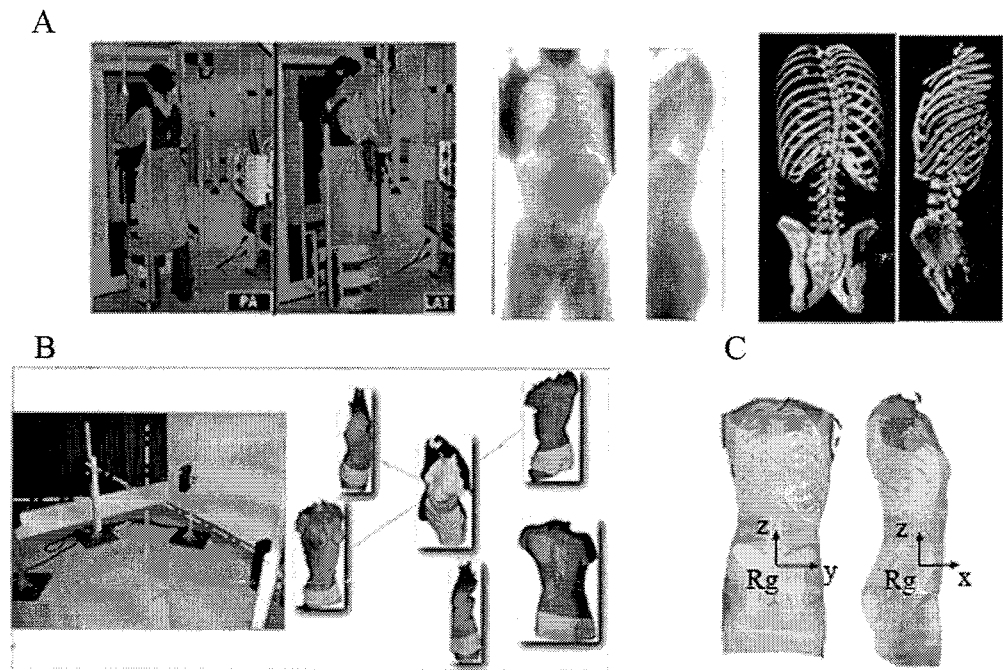


Figure 1. **A**, Acquisition of the internal geometry using the multiview radiographic reconstruction technique. **B**, Acquisition of the external geometry using topography technique. **C**, Superimposition of the 2 geometries.

epiphyses compared with the forces acting in an upright posture.

## Materials and Methods

### Patient-Specific Model Geometry

The geometry of the spine, rib cage, and pelvis of 2 scoliotic patients (P1 and P2) were acquired using a multiview self-calibrated radiography reconstruction technique<sup>15-17</sup> (Figure 1A). On 3 radiographs (lateral, posteroanterior, and posteroanterior with a 20° angled down incidence) anatomic landmarks (6 per vertebra, 11 per rib, and 24 for the pelvis) were digitized and reconstructed in 3-dimension. An atlas of detailed reconstructed vertebrae, ribs, and pelvis along with a free-form interpolation technique were then used to obtain the final geometry.<sup>16</sup> The accuracy of this reconstruction method was 3.3 mm on average (SD 3.8 mm).<sup>16</sup> In addition, the external trunk surface of the patient was digitized using a 3-dimensional surface topography technique (3-dimensional Capturor; Inspec Inc., Montreal, Quebec, Canada)<sup>18</sup> (Figure 1B). Twelve markers were attached to the patient's torso and were visible on both the radiographs and the trunk surface. Internal and external geometries were superimposed by applying a point-to-point least square algorithm to the respective sets of 12 markers (Figure 1C).<sup>19</sup> A global coordinate system Rg, with origin at the center of the first sacral vertebra S1, was associated with this geometry such that the z-axis was directed vertically upward, the x-axis was posteroanterior, and the y-axis was lateral (oriented from left to right; Figure 1). The 2 scoliotic patients had a right thoracic (Cobb: 36° and 20°, respectively) and a left lumbar curve (Cobb: 16° and 33°, respectively; Figure 4).

### Patient-Specific Finite Element Model of the Trunk

Based on this geometry, a personalized FE model of the patient's torso was built. The Ansys 11.0 FE package (Ansys Inc., Canonsburg, PA) was used. It has been presented in previous publications<sup>9,14,20,21</sup> (Figure 3). The thoracic and lumbar vertebrae, intervertebral discs, ribs, sternum, cartilage, and abdominal cavity were represented by 3-dimensional elastic beam

elements, the zygapophysial joints by shells and surface-to-surface contact elements, the vertebral and intercostal ligaments by tension-only spring elements, and the external soft tissues by hexahedron elements.

Mechanical properties of all the components of the model were taken from experimental and published data.<sup>10,20,21</sup> To evaluate the influence of the flexibility of the spine, a "stiff" and a "flexible" spine were tested (intervertebral disc stiffness multiplied and divided by 2, respectively).<sup>22</sup>

Nodes representing the center of gravity of each trunk slice corresponding to a vertebral level were created. Their position in the sagittal plane was derived from the literature<sup>23-26</sup> and scaled according to patient size. In the coronal plane, it has been assumed that their position followed the scoliotic curve of the spine. Nondeformable beam elements connected these nodes to their relative vertebra to transmit the gravitational forces to the spine. The magnitude of the gravitational forces associated with each center of gravity node was scaled to the patient's specific weight based on published values.<sup>23-26</sup>

### Supine Bending Simulation

The initial geometry of the patients was acquired while they were standing (under gravity). A simulation was first done to compute the transition from standing to supine position (Figure 2). Forces directed vertically upward were applied to find the zero-gravity geometry (Figure 2B). During this step, the pelvis was fixed in space and the translation of the first thoracic vertebra in the transverse plane was blocked. An optimization process was developed to find the zero-gravity geometry (stress free) that leads, when the vertical gravitational forces are reapplied, to the actual geometry of the patient in the standing position (Figure 2C). Gravitational forces were then applied in the anteroposterior direction to find the geometry of the patient in the supine position (Figure 2D). During this step, the pelvis was fixed in space, the translation of the first thoracic vertebra in the transverse plane was blocked, and the translation of the seventh and eighth ribs in the anteroposterior direction (x-axis)

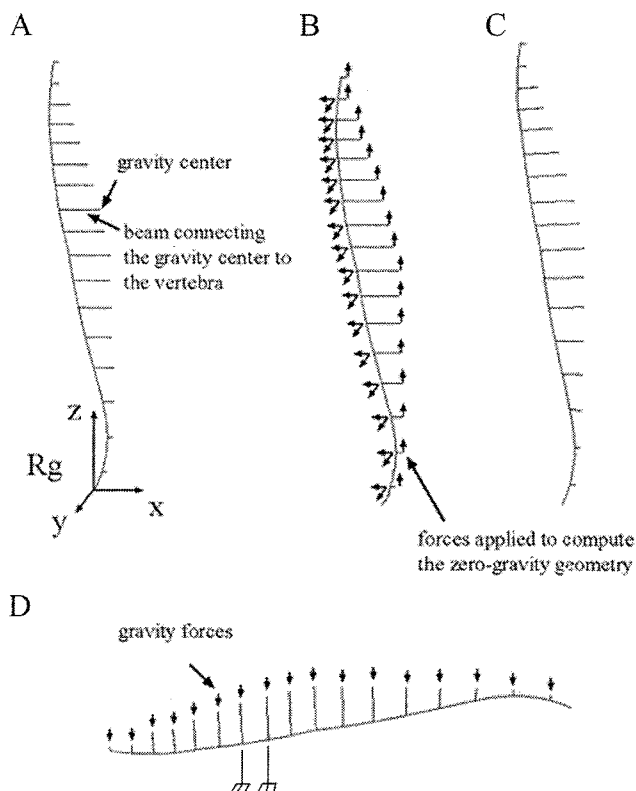


Figure 2. Simulation of the supine position. **A**, Initial geometry of the patient's spine in the standing position. **B**, Computation of the zero-gravity geometry. **C**, Zero-gravity geometry. **D**, Computation of the supine position.

was blocked (to simulate supine positioning on a horizontal surface).

From this supine position (Figure 3A), lateral bending was simulated by applying a displacement of 150 mm to the first thoracic vertebra (Figure 3B). For P1, the major curve is the right thoracic curve, and thus, the bending was in the right direction, whereas for P2 the major curve is the left lumbar curve, and thus, the bending was in the left direction.

**Brace Model**

A custom-fit geometrical brace model following the Charleston brace system principles was created over the already generated FEM of the patient trunk (Figure 3C). It was based on 10 generative curves whose shape was determined by 24 geometrical

parameters computed on the external surface of the patient in the simulated supine bending position. A surface interpolating these 10 generative curves was created. It was divided into 170 subsurfaces. The brace openings were created by deleting some subsurfaces. The remaining subsurfaces were then extruded outward to create a volumetric representation of the foam layer of the brace geometry. The pads were created by inwardly extruding some subsurfaces.

The modeled pads were positioned on the right thoracic region, on the left lumbar region, and on the trochanter extension for both patients. For P1, the trochanteric extension was located on the left side whereas it was located on the right side for P2. The external rigid shell followed the sagittal curves of the patient in the sagittal plane.

The FE model of the brace was then generated. An external rigid shell was located on the external surface of the volume representing the foam layer, and was modeled by 4-node quadrilateral shell elements. The foam layer and the pads were modeled by 8-nodes hexahedral elements (Figure 3D). The material of the rigid shell was polyethylene ( $E = 1500 \text{ Mpa}$ ,  $\nu = 0.3$ ), the foam layer was made of soft polyethylene foam ( $E = 1 \text{ Mpa}$ ,  $\nu = 0.3$ ), and the pads were represented by stiff polyethylene foam ( $E = 10 \text{ Mpa}$ ,  $\nu = 0.3$ ).<sup>21,27</sup> These materials were modeled as linear elastic. A surface-to-surface contact interface taking friction into account ( $\mu = 0.6^{28}$ ) was created between the interior of the brace model and the exterior of the trunk model.

**Simulation of the Brace Installation**

The brace installation on the patient was simulated in 2 steps after that the supine bending position was obtained as described previously. In the first step, the brace was opened by applying displacements on 4 nodes located in its anterior part and was positioned on the patient. In the second step, 3 sets of collinear forces representing thoracic, lumbar, and pelvic strap tensions of 60 N were applied on the nodes corresponding to the strap fixations on the anterior part of the brace (Figure 3E).<sup>29</sup> Finally, the displacement initially applied to T1 was suppressed, and the equilibrium state was computed.

**Study of Brace Biomechanics**

Once the simulation was completed, several 3-dimensional clinical indexes (Cobb angles, kyphosis, lordosis, rib hump, and axial rotation) and the pressures generated by the brace on the patient's trunk were computed. The global forces and moments acting on the vertebral endplates and the axial compressive stresses in the spine were also evaluated in a local system  $R_{local}$  for each vertebra. The origin of  $R_{local}$  was located at the

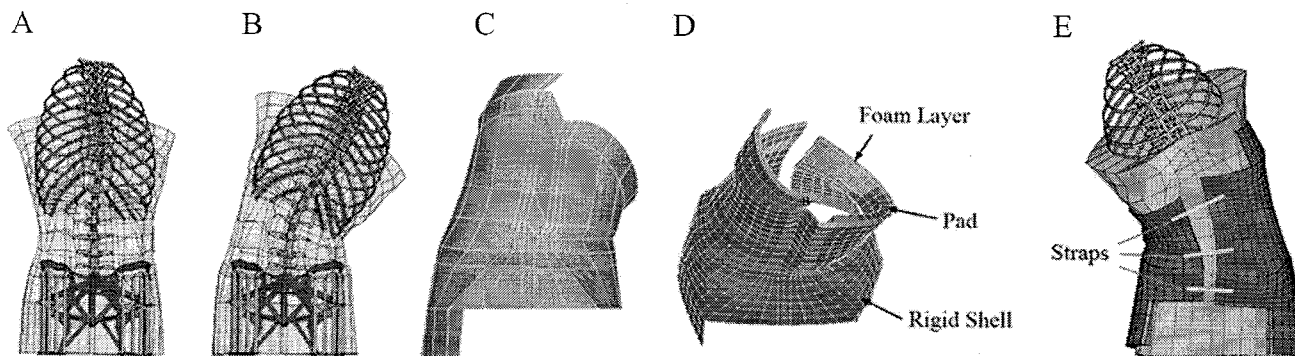


Figure 3. **A**, FEM of the patient (P1) in the supine position. **B**, FEM in the supine bending position. **C**, Geometrical model of the brace. **D**, FEM of the brace. **E**, Resulting FEM (brace installed on the patient).

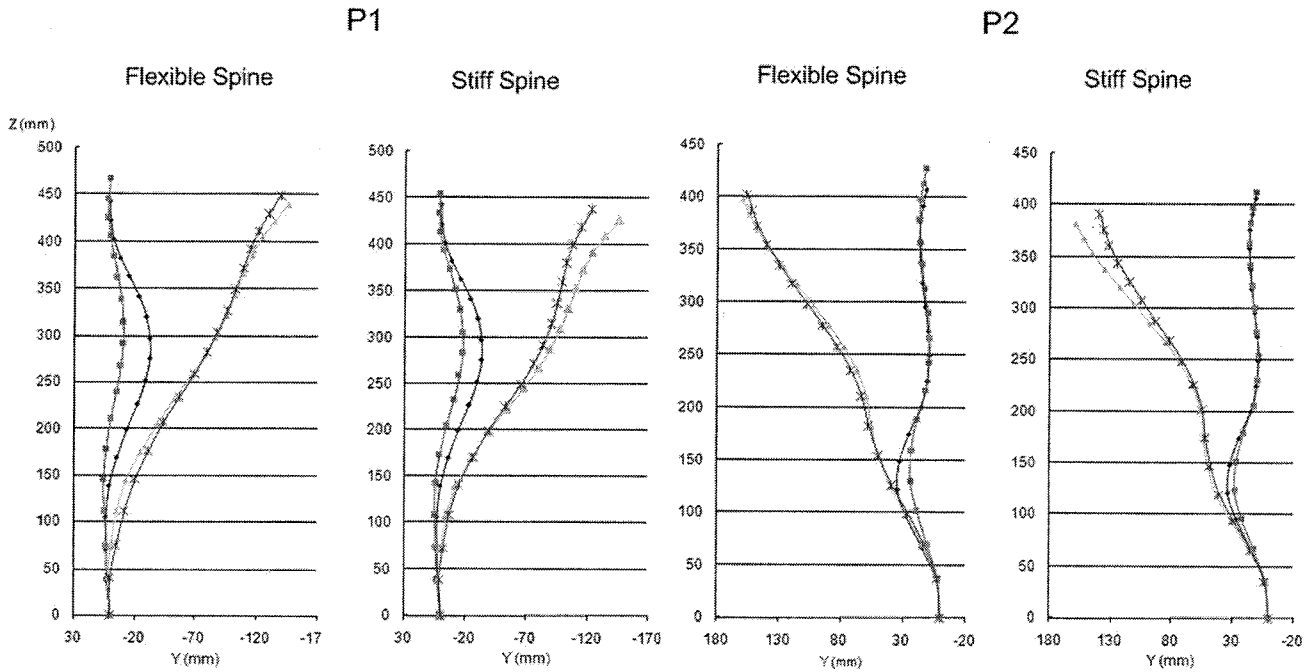


Figure 4. Spine curves of the patients in the coronal plane. (◆), Initial standing position. (■) Simulated supine position. (▲), Simulated supine bending. (\*), Simulated in brace.

center of the vertebral body. The z-axis was in the direction of the line joining the centers of the vertebral endplate centers. The x-axis was the projection of the global x-axis on the plane perpendicular to the z-axis. The y-axis was perpendicular to the x- and z-axes.

■ Results

The transition from an upright to supine position induced a mean 38% correction of the lumbar and thoracic Cobb angle (Figure 4 and Table 1). The transition from a straight supine position to a bent supine position in brace induced a further reduction (mean, 37%) of the major scoliotic curves (thoracic for P1 and lumbar for P2) but also increased the secondary curve (mean, 25%). The

correction in the transverse plane was negligible (axial rotation of the apical vertebra and of the rib hump).

The simulated brace exerted pressure on the torso of the patients against the left lumbar pad (Figure 5A), the right thoracic pad (Figure 5B), the trochanteric pads (Figure 5C), and the abdominal shell (Figure 5D). Brace-torso interface pressure ranged between 0 and 30 kPa.

The resulting local side-bending moments (Mx) applied on the vertebral endplates in the standing and supine positions and in brace are shown in Figure 7. This bending moment quantifies the asymmetrical compressive loading of the vertebrae in the coronal plane shown in Figure 6. For the patients in an upright standing position, the compressive loading of the spine in the coronal plane is asymmetrical and maximal at the apical levels. The compressive loading is greater in the concavity of the scoliotic curves (compression up to 1 MPa for P1 and P2) than in their convexity (tension up to 0.5 MPa for P1 and 0.2 MPa for P2). A marked asymmetrical compressive pressure is also present at L5 for P2, with a greater compression on the left than on the right side.

In the supine position, this asymmetrical loading becomes almost null. In the Charleston brace, the side of the spine located in the direction of the bending (right for P1 and left for P2) is subjected to compressive stresses (up to 1 MPa) whereas the other side is subjected to tensile stresses (up to 1 MPa). Consequently, the Charleston brace induced an inverted bending moment on the major scoliotic curve compared with the upright standing position. It, however, generated bending moments on the secondary curve similar to those present in the upright standing position. For P1, this side effect was

Table 1. Geometric Indices of the Patients in Different Positions

	Flexible Spine			Stiff Spine	
	Standing	Supine	In Brace	Supine	In Brace
<b>P1</b>					
Thoracic Cobb (°)	36	15	6	21	13
Lumbar Cobb (°)	16	7	12	10	17
Kyphosis (°)	9	1	1	3	4
Lordosis (°)	37	25	22	30	29
Rib hump (°)	20	18	21	18	21
Axial rotation (°)	10	10	10	10	10
<b>P2</b>					
Thoracic Cobb (°)	20	14	15	17	21
Lumbar Cobb (°)	33	19	1	25	9
Kyphosis (°)	49	29	31	36	38
Lordosis (°)	37	23	26	28	30
Rib hump (°)	9	9	9	9	9
Axial rotation (°)	10	9	11	10	11

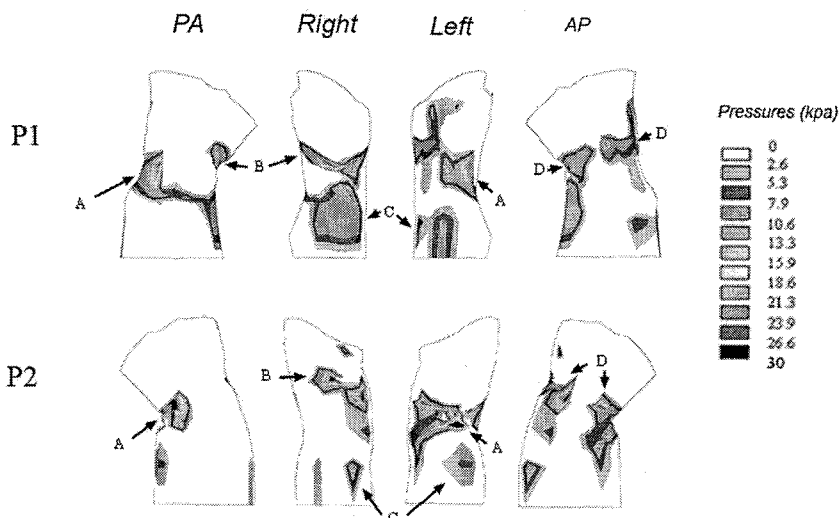


Figure 5. Simulated pressures exerted by the braces on the patient torsos against the left lumbar pad (A), the right thoracic pad (B), the trochanteric pads (C), and the abdominal shell (D).

equivalent in magnitude to the effect on the major curve. For P2, it remained inferior (Figure 7).

■ Discussion

The resulting geometrical corrections given by the model corresponded to the expected clinical behavior and to the published experimental data. The transition from standing to supine position induced a correction of the scoliotic curves (Table 1, Figure 4) because of the suppression of gravity forces along the spine longitudinal axis and the interaction with the horizontal surface. The amount of

reduction of the coronal curves is similar to the mean reduction of 37% found by Delorme *et al*<sup>30</sup> in prone position of surgical patients. The relative correction of the major scoliotic curve obtained in-brace (between 58% and 92% for P1 and between 58% and 97% for P2 compared with the standing position) is similar to the published data (mean correction of 73%–83%<sup>1,7</sup> for the primary curve with the Charleston brace system<sup>1,7</sup>).

The distribution of the pressures exerted by the braces on the patients' trunk (Figure 5) corresponded to what was expected considering the positioning of the pads.

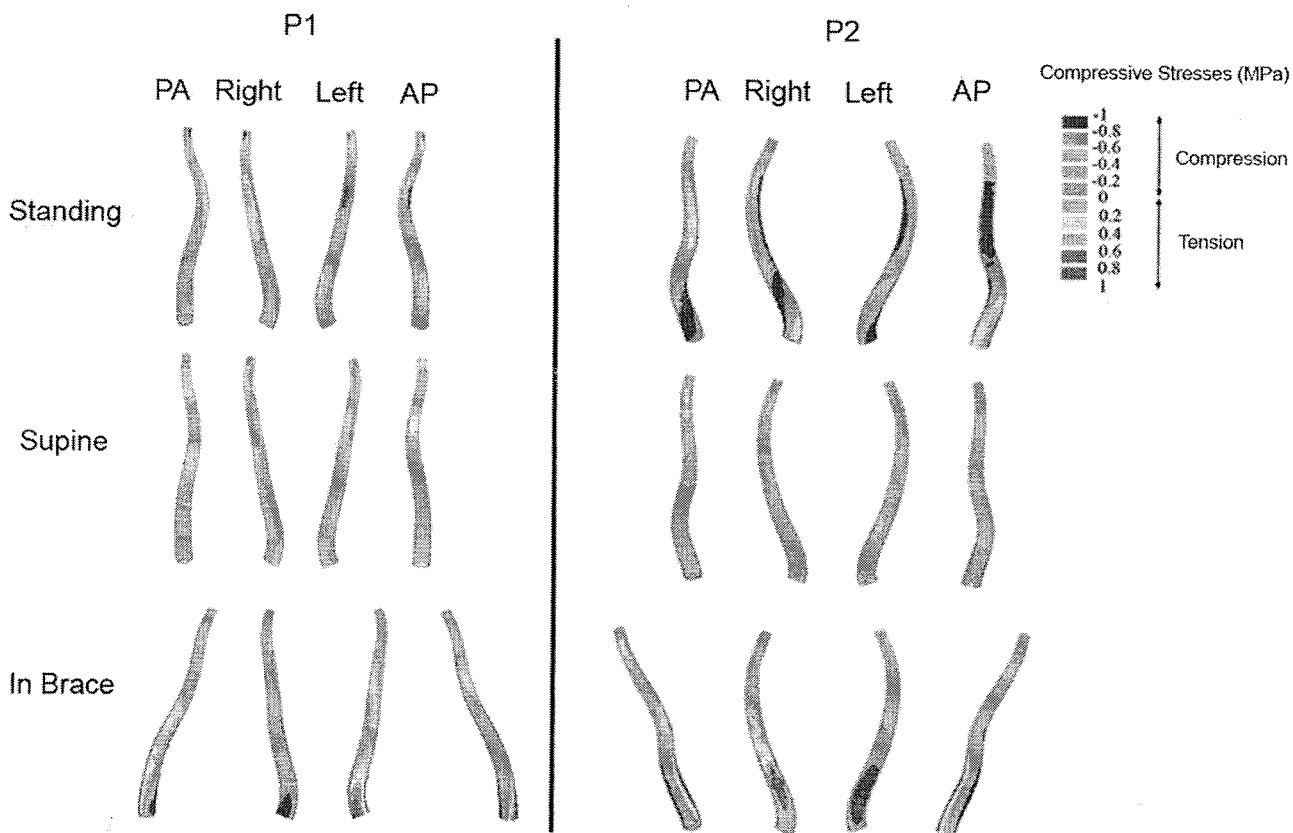


Figure 6. Compressive stresses in the spine models (stiff spine model).

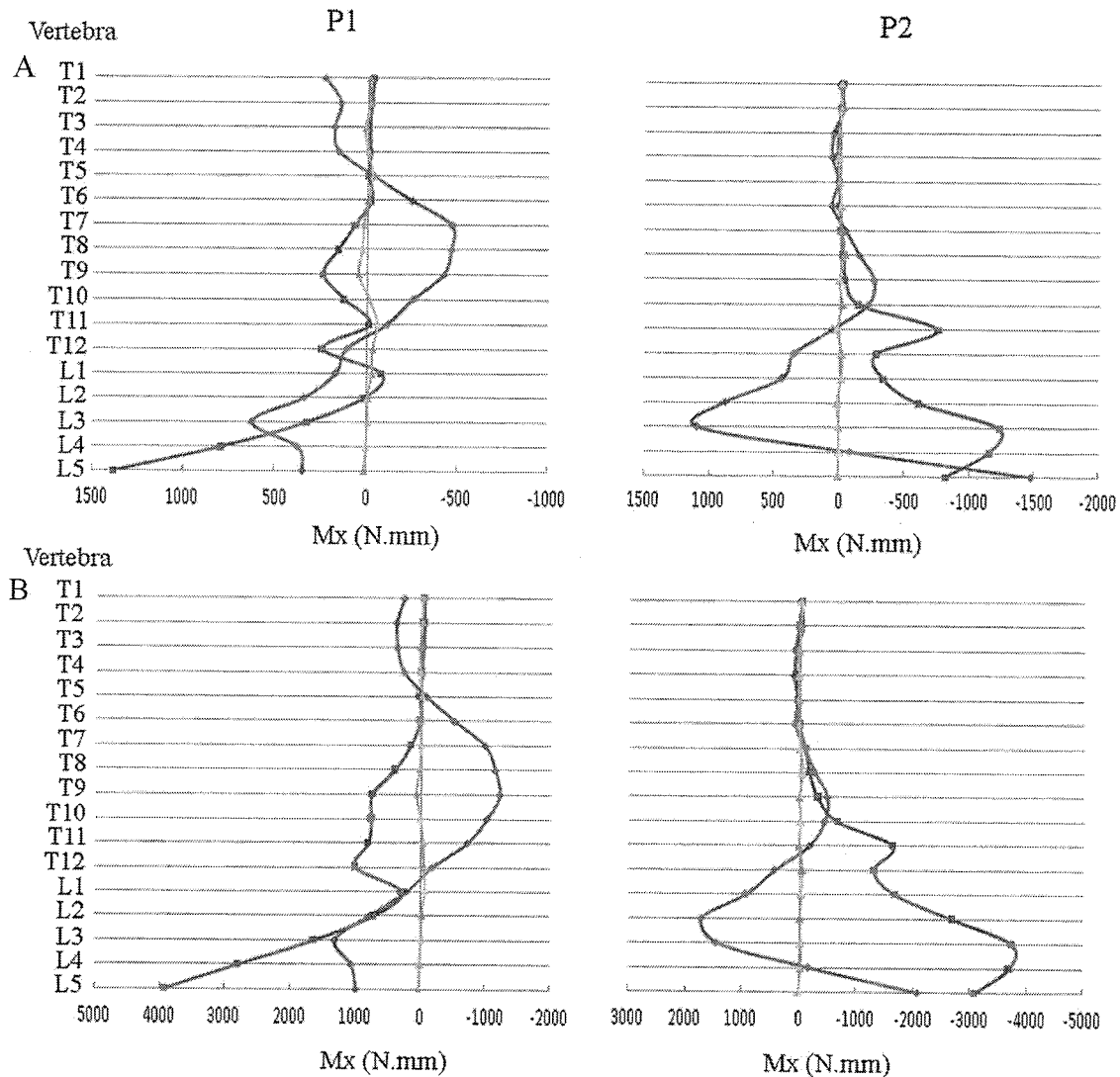


Figure 7. Resulting bending moment,  $M_x$ , on the vertebral endplates. (◆), Initial standing position. (▲), Simulated supine position. (■), Simulated supine position wearing the brace. **A**, Flexible spine. **B**, Stiff spine.

The pressure, between 10 and 30 kPa, corresponded to experimental measures reported by Mac-Thiong *et al*<sup>29</sup> with the Boston brace system. The action of the thoracic, lumbar, and trochanteric pads was clearly visible. The pressures are the results of force-reaction because of the interaction of 2 deformable bodies with their specific stiffness (patient's trunk and brace system) and should not be interpreted as external forces applied on the torso.<sup>20</sup>

Globally, the biomechanical action of the Charleston brace on the asymmetrical compressive loading of the vertebrae in the coronal plane corresponded to what was assumed by its designers.<sup>2</sup> For the major curve, the Charleston brace induced an asymmetrical loading of the vertebral endplates in the coronal plane inverted relatively to the standing position (Figures 6 and 7), with compressive stresses in the convexity of the curve and tensile stresses in the concavity. According to the Hueter-Volkman principle<sup>31</sup> (compressive stresses slow growth whereas tensile stresses fasten growth) it should invert the growth deformation process of the major scoliotic

curve. However, the Charleston brace also generated negative effects for the compensatory curves (especially for P1). Asymmetrical loads of the vertebrae were similar to those in the standing position. This could aggravate the deformation process of the secondary curves. It confirms the assertions of Price *et al*<sup>1,3</sup> who recommended to carefully follow the evolution of the compensatory curves when using the Charleston brace.

The interpretation of growth modulation effects should be done with caution. The growth sensitivity to mechanical stresses and mechanoregulation are still not well understood and are the subject of active research.<sup>32-36</sup> It is not well known whether there exists a threshold load that could trigger the growth modulation process, or what is the most efficient load condition (static *vs.* dynamic).<sup>35,36</sup> The circumdiurnal effectiveness of the growth modulation process is also questioned, but Stokes *et al*<sup>37</sup> concluded that there was no difference in growth modulation between diurnal and nocturnal periods.

When interpreting the results of this study, the model limits should also be taken into account. The trunk model did not include muscles. However, their role is probably passive during the night while the patient is asleep. With the model, it was possible to maintain the supine bending position with very low forces at the boundary condition sites in the coronal and sagittal planes. The intervertebral discs and vertebrae were represented by beam elements without taking into account the hydrostatic behavior of the nucleus, which might affect the load distribution on the growth plates. Future work should focus on using a more detailed model of the spine to analyze this effect. Even if the results are quite plausible compared with published literature,<sup>32,38</sup> there is still no data about the stress distribution in a scoliotic spine, which makes the validation quite difficult.<sup>38,39</sup>

The next step of this project will be to validate more thoroughly the model by simulating the Charleston brace effect on a larger cohort of patients that actually wear a Charleston brace (and compare the simulation results to the in-brace correction). Supine and bending radiographs acquisition and calibrated flexibility tests could also be included in the protocol to personalize the mechanical properties of the spine model for each patient and to validate the intermediate steps of the simulation process.<sup>22,40</sup>

This study showed the feasibility of simulating the Charleston brace and the value of the model in providing insights into its biomechanical action. It confirmed the working principle of the brace assumed by its designers,<sup>2</sup> which consists of inverting the asymmetrical compressive loading at the level of the major scoliotic curve. It also highlighted a shortcoming of the supine side-bending principle, which is to worsen the asymmetrical compressive loading in the compensatory curves. The FE model developed could help studying different brace designs and to optimize brace efficiency.

#### ■ Key Points

- Charleston brace's immediate effect can be simulated.
- The brace inverts the asymmetrical compressive loading in the major scoliotic curve.
- It worsens the asymmetrical compressive loading in the compensatory curve.

#### Acknowledgment

The authors thank Dr. Archana Sangole, PhD, for the careful revision of the manuscript.

#### References

1. Price CT, Scott DS, Reed FE Jr, et al. Nighttime bracing for adolescent idiopathic scoliosis with the Charleston bending brace. Preliminary report. *Spine* 1990;15:1294-9.
2. Hooper R, Reed F, Price C. The Charleston brace. SRS bracing manual. Available at: [http://www.srs.org/professionals/bracing\\_manuals/](http://www.srs.org/professionals/bracing_manuals/). 2003.
3. Price CT, Scott DS, Reed FR Jr, et al. Nighttime bracing for adolescent idiopathic scoliosis with the Charleston bending brace: long-term follow-up. *J Pediatr Orthop* 1997;17:703-7.
4. Trivedi JM, Thomson JD. Results of Charleston bracing in skeletally immature patients with idiopathic scoliosis. *J Pediatr Orthop* 2001;21:277-80.
5. Gepstein R, Leitner Y, Zohar E, et al. Effectiveness of the Charleston bending brace in the treatment of single-curve idiopathic scoliosis. *J Pediatr Orthop* 2002;22:84-7.
6. Howard A, Wright JG, Hedden D. A comparative study of TLSO, Charleston, and Milwaukee braces for idiopathic scoliosis. *Spine* 1998;23:2404-11.
7. Katz DE, Richards BS, Browne RH, et al. A comparison between the Boston brace and the Charleston bending brace in adolescent idiopathic scoliosis. *Spine* 1997;22:1302-12.
8. Andriacchi TP, Schultz AB, Belytschko TB, et al. Milwaukee brace correction of idiopathic scoliosis. A biomechanical analysis and a retrospective study. *J Bone Joint Surg Am* 1976;58:806-15.
9. Perie D, Aubin CE, Petit Y, et al. Boston brace correction in idiopathic scoliosis: a biomechanical study. *Spine* 2003;28:1672-7.
10. Perie D, Aubin CE, Petit Y, et al. Personalized biomechanical simulations of orthotic treatment in idiopathic scoliosis. *Clin Biomech (Bristol, Avon)* 2004;19:190-5.
11. Gignac D, Aubin CE, Dansereau J, et al. Optimization method for 3D bracing correction of scoliosis using a finite element model. *Eur Spine J* 2000;9:185-90.
12. Patwardhan AG, Bunch WH, Meade KP, et al. A biomechanical analog of curve progression and orthotic stabilization in idiopathic scoliosis. *J Biomech* 1986;19:103-17.
13. Wynarsky GT, Schultz AB. Optimization of skeletal configuration: studies of scoliosis correction biomechanics. *J Biomech* 1991;24:721-32.
14. Clin J, Aubin CE, Labelle H. Virtual prototyping of a brace design for the correction of scoliotic deformities. *Med Biol Eng Comput* 2007;45:467-73.
15. Aubin CE, Descrimes JL, Dansereau J, et al. [Geometrical modeling of the spine and the thorax for the biomechanical analysis of scoliotic deformities using the finite element method]. *Ann Chir* 1995;49:749-61.
16. Delorme S, Petit Y, de Guise JA, et al. Assessment of the 3-D reconstruction and high-resolution geometrical modeling of the human skeletal trunk from 2-D radiographic images. *IEEE Trans Biomed Eng* 2003;50:989-98.
17. Kadoury S, Cheriet F, Dansereau J, et al. Three-dimensional reconstruction of the scoliotic spine and pelvis from uncalibrated biplanar x-ray images. *J Spinal Disord Tech* 2007;20:160-7.
18. Pazos V, Cheriet F, Dansereau J, et al. Reliability of trunk shape measurements based on 3-D surface reconstructions. *Eur Spine J* 2007;16:1882-91.
19. Fortin D, Cheriet F, Beausejour M, et al. A 3D visualization tool for the design and customization of spinal braces. *Comput Med Imaging Graph* 2007;31:614-24.
20. Aubin CE, Dansereau J, de Guise JA, et al. [A study of biomechanical coupling between spine and rib cage in the treatment by orthosis of scoliosis]. *Ann Chir* 1996;50:641-50.
21. Perie D, Aubin CE, Lacroix M, et al. Biomechanical modelling of orthotic treatment of the scoliotic spine including a detailed representation of the brace-torso interface. *Med Biol Eng Comput* 2004;42:339-44.
22. Petit Y, Aubin CE, Labelle H. Patient-specific mechanical properties of a flexible multi-body model of the scoliotic spine. *Med Biol Eng Comput* 2004;42:55-60.
23. Cheng CK, Chen HH, Chen CS, et al. Segment inertial properties of Chinese adults determined from magnetic resonance imaging. *Clin Biomech (Bristol, Avon)* 2000;15:559-66.
24. Liu YK, Laborde JM, Van Buskirk WC. Inertial properties of a segmented cadaver trunk: their implications in acceleration injuries. *Aerosp Med* 1971;42:650-7.
25. Pearsall DJ, Reid JG, Livingston LA. Segmental inertial parameters of the human trunk as determined from computed tomography. *Ann Biomed Eng* 1996;24:198-210.
26. Pearsall DJ, Reid JG, Ross R. Inertial properties of the human trunk of males determined from magnetic resonance imaging. *Ann Biomed Eng* 1994;22:692-706.
27. Sanders JE, Greve JM, Mitchell SB, et al. Material properties of commonly-used interface materials and their static coefficients of friction with skin and socks. *J Rehabil Res Dev* 1998;35:161-76.
28. Zhang M, Mak AF. In vivo friction properties of human skin. *Prosthet Orthot Int* 1999;23:135-41.
29. Mac-Thiong JM, Petit Y, Aubin CE, et al. Biomechanical evaluation of the Boston brace system for the treatment of adolescent idiopathic scoliosis: relationship between strap tension and brace interface forces. *Spine* 2004;29:26-32.
30. Delorme S, Labelle H, Poitras B, et al. Pre-, intra-, and postoperative three-dimensional evaluation of adolescent idiopathic scoliosis. *J Spinal Disord* 2000;13:93-101.

31. Roaf R. Vertebral growth and its mechanical control. *J Bone Joint Surg Br* 1960;42:40–59.
32. Stokes IA, Aronsson DD, Dimock AN, et al. Endochondral growth in growth plates of three species at two anatomical locations modulated by mechanical compression and tension. *J Orthop Res* 2006;24:1327–34.
33. Villemure I, Chung MA, Seck CS, et al. Static compressive loading reduces the mRNA expression of type II and X collagen in rat growth-plate chondrocytes during postnatal growth. *Connect Tissue Res* 2005;46:211–9.
34. Villemure I, Cloutier L, Matyas JR, et al. Non-uniform strain distribution within rat cartilaginous growth plate under uniaxial compression. *J Biomech* 2007;40:149–56.
35. Frost HM. Skeletal structural adaptations to mechanical usage (SATMU): 3. The hyaline cartilage modeling problem. *Anat Rec* 1990;226:423–32.
36. Frost HM. Skeletal structural adaptations to mechanical usage (SATMU): 1. Redefining Wolff's law: the bone modeling problem. *Anat Rec* 1990;226:403–13.
37. Stokes IA, Gwadera J, Dimock A, et al. Modulation of vertebral and tibial growth by compression loading: diurnal versus full-time loading. *J Orthop Res* 2005;23:188–95.
38. Meir AR, Fairbank JC, Jones DA, et al. High pressures and asymmetrical stresses in the scoliotic disc in the absence of muscle loading. *Scoliosis* 2007;2:4.
39. Meir A, McNally DS, Fairbank JC, et al. The internal pressure and stress environment of the scoliotic intervertebral disc—a review. *Proc Inst Mech Eng [H]* 2008;222:209–19.
40. Lamarre ME, Parent S, Labelle H, et al. Assessment of spinal flexibility in adolescent idiopathic scoliosis: suspension versus side-bending radiography. *Spine* 2009;34:591–7.